Science Advances
AAAS

advances.sciencemag.org/cgi/content/full/6/44/eabc6601/DC1

Supplementary Materials for

Layer-engineered large-area exfoliation of graphene

Ji-Yun Moon, Minsoo Kim, Seung-Il Kim, Shuigang Xu, Jun-Hui Choi, Dongmok Whang, Kenji Watanabe, Takashi Taniguchi, Dong Seop Park, Juyeon Seo, Sung Ho Cho*, Seok-Kyun Son*, Jae-Hyun Lee*

*Corresponding author. Email: sunho19.cho@samsung.com (S.H.C.); skson@mokpo.ac.kr (S.-K.S.); jaehyunlee@ajou.ac.kr (J.-H.L.)

Published 28 October 2020, *Sci. Adv.* **6**, eabc6601 (2020)
DOI: 10.1126/sciadv.abc6601

This PDF file includes:

Note S1
Figs. S1 to S14
References

note S1. Raman analysis

We can extract the contributions of the strain and doping effect for a given point with the analysis method proposed by LEE et al (*26*). The model consists of two vectors: $\mathbf{OP}=a\boldsymbol{e}_{\mathbf{T}} + b\boldsymbol{e}_{\mathbf{H}}$, where a and b are constants, and $\boldsymbol{e}_{\mathbf{T}}$ and $\boldsymbol{e}_{\mathbf{H}}$ are unit vector components for tensile strain and hole doping effects, respectively (here, the initial values of $\boldsymbol{e}_{\mathbf{T}}$ =2.2 and $\boldsymbol{e}_{\mathbf{H}}$ =0.7 were used). We assumed that the intrinsic frequencies of the G and 2D peaks of 1582 cm^{-1} and 2677 cm^{-1}, respectively, were not affected by extra charge and strain. Note that we cannot observe a clear linearity caused by charge doping (0.75 for holes and 0.44 for electrons) in graphene prepared by Au-LEE. Therefore, we conclude that the linear variations in ω_G and ω_{2D} are due to the native strain in graphene.

Supplementary Figures

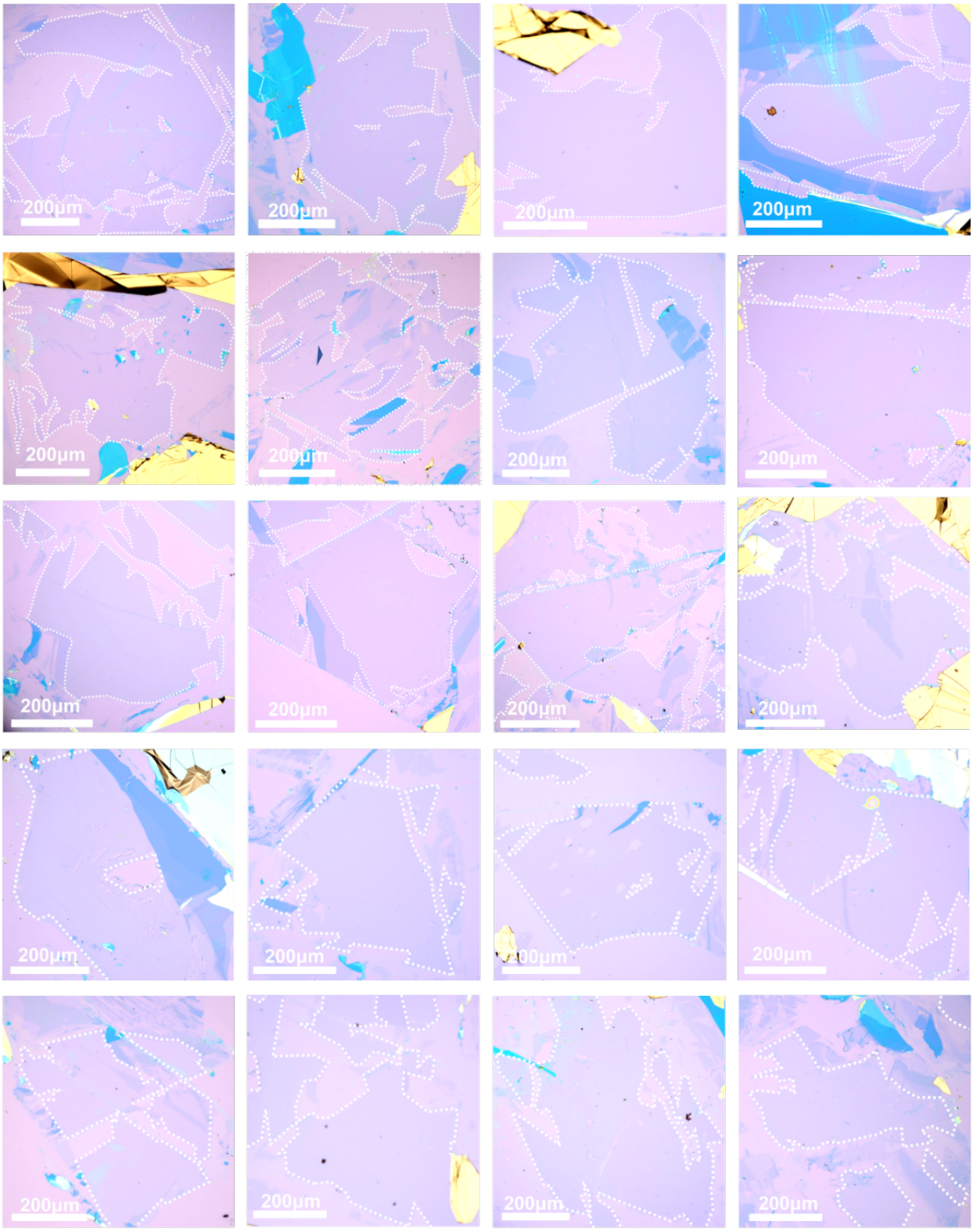

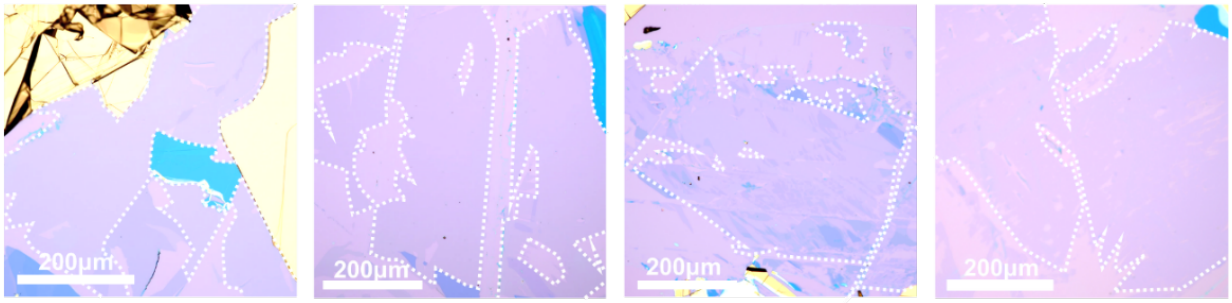

Fig. S1 OM images of Au-LEE-graphene. Twenty-four samples of large-area monolayer graphene produced by the LEE method on 300 nm SiO_2/Si substrates. The average size of exfoliated graphene is similar to that of the atomically flat domains of the mother graphite, as shown in Fig. 1 and fig. S2. Most of the cracks in exfoliated graphene existed at the domain boundaries because transferred LEE-graphene could not conformally contact with target substrate. Therefore, we believe that the size of exfoliated graphene could be even larger and crackless, towards the wafer scale, if we prepare large-scale and flat graphite on rigid substrate (e.g., CVD-grown multilayer graphene on wafer).

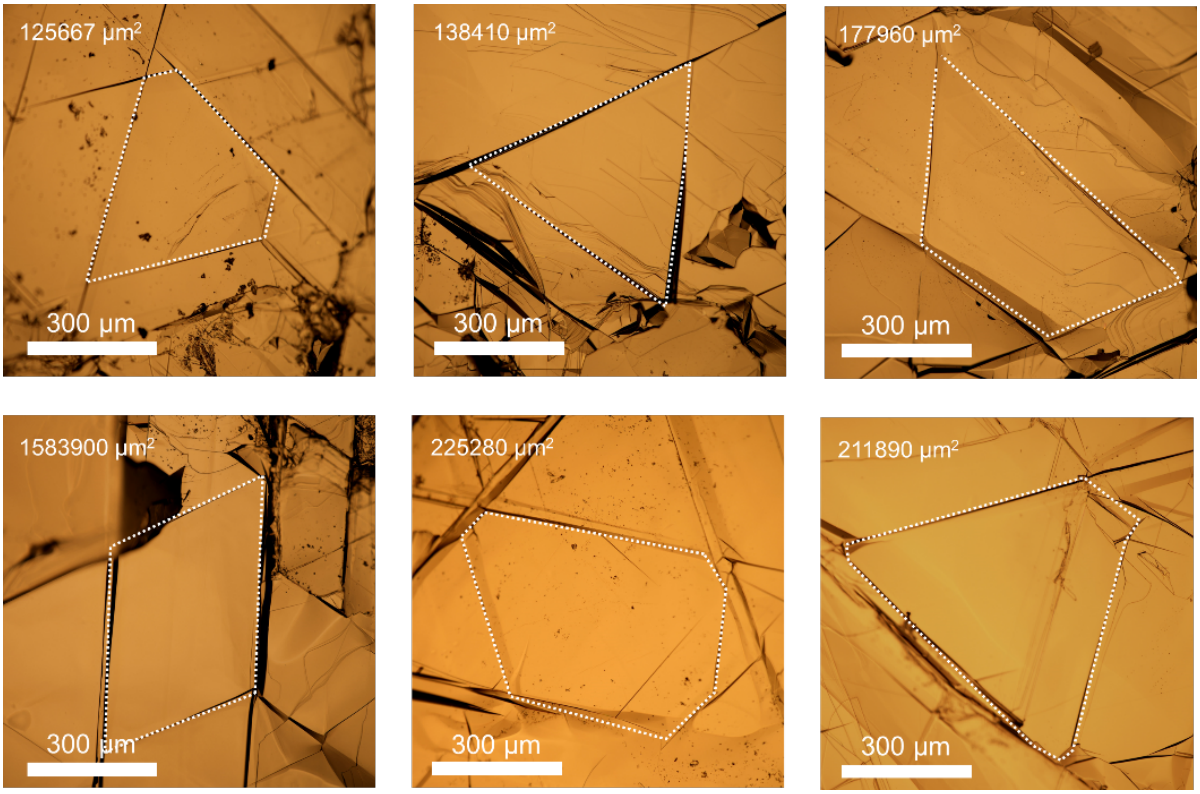

Fig. S2 OM images of the cleaved natural graphite surface. The size and area of individual domain is analogous to those of LEE-graphene. The calculated areas of flat domains are written on the top left in each image.

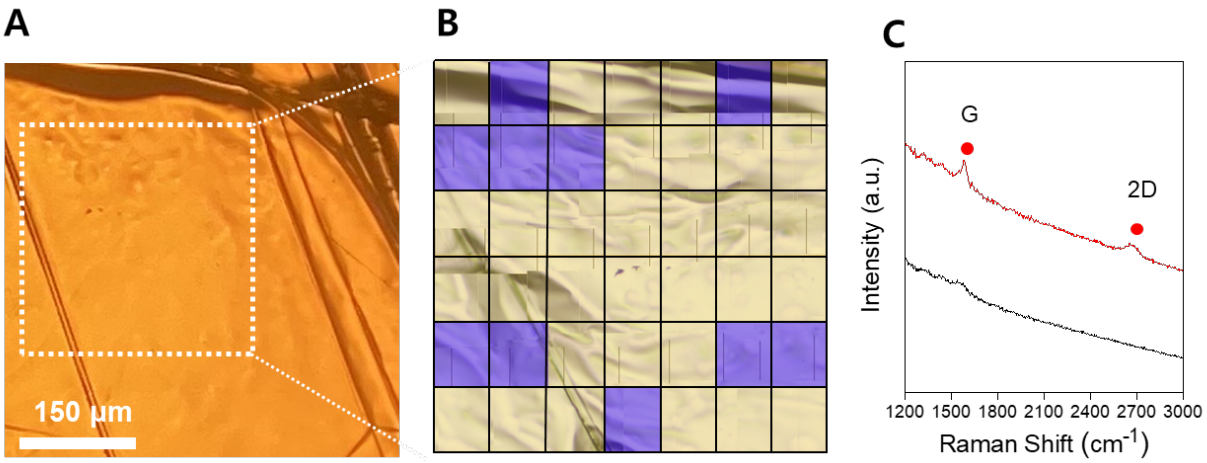

Fig. S3 Non-spalling area on the surface of Au film. (A) Surface-OM image of the exfoliated Au film from natural graphite. (B) Raman mapping image is overlaid onto the white box in (A). The purple areas indicates the presence of graphene. Individual spectrum was acquired with 40 μm steps along the X- and Y-axis. (C) Representative Raman spectra of the exfoliated Au film with graphene (red) or without graphene (black).

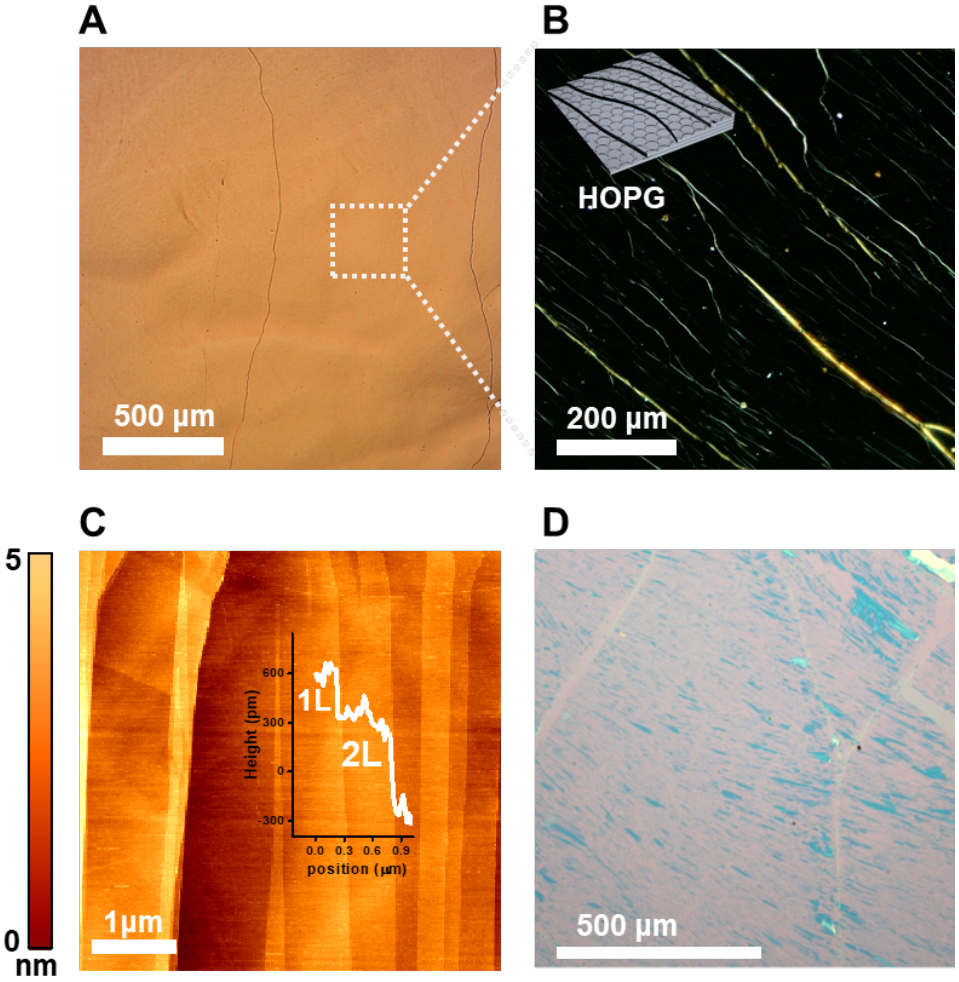

Fig. S4 Surface morphology of HOPG. To analyze the surface morphology of HOPG, we used OM (both bright field (BF) and dark field (DF) modes) and AFM. (**A-C**) The surface of HOPG consists of large domains with lateral sizes of 1-2 mm or more, but each domain consists of step edges that naturally occur during mechanical cleavage. These step edges consist of 1-3 layers and are aligned in one direction according to AFM analysis. The root mean square value of the HOPG surface was measured to be 0.42 nm. (**D**) As a result of applying the LEE method to HOPG flakes, a discontinuous monolayer is obtained over the entire area, and bi- and tri-layers are also present because crack propagation easily occurs at the step edges present in HOPG.

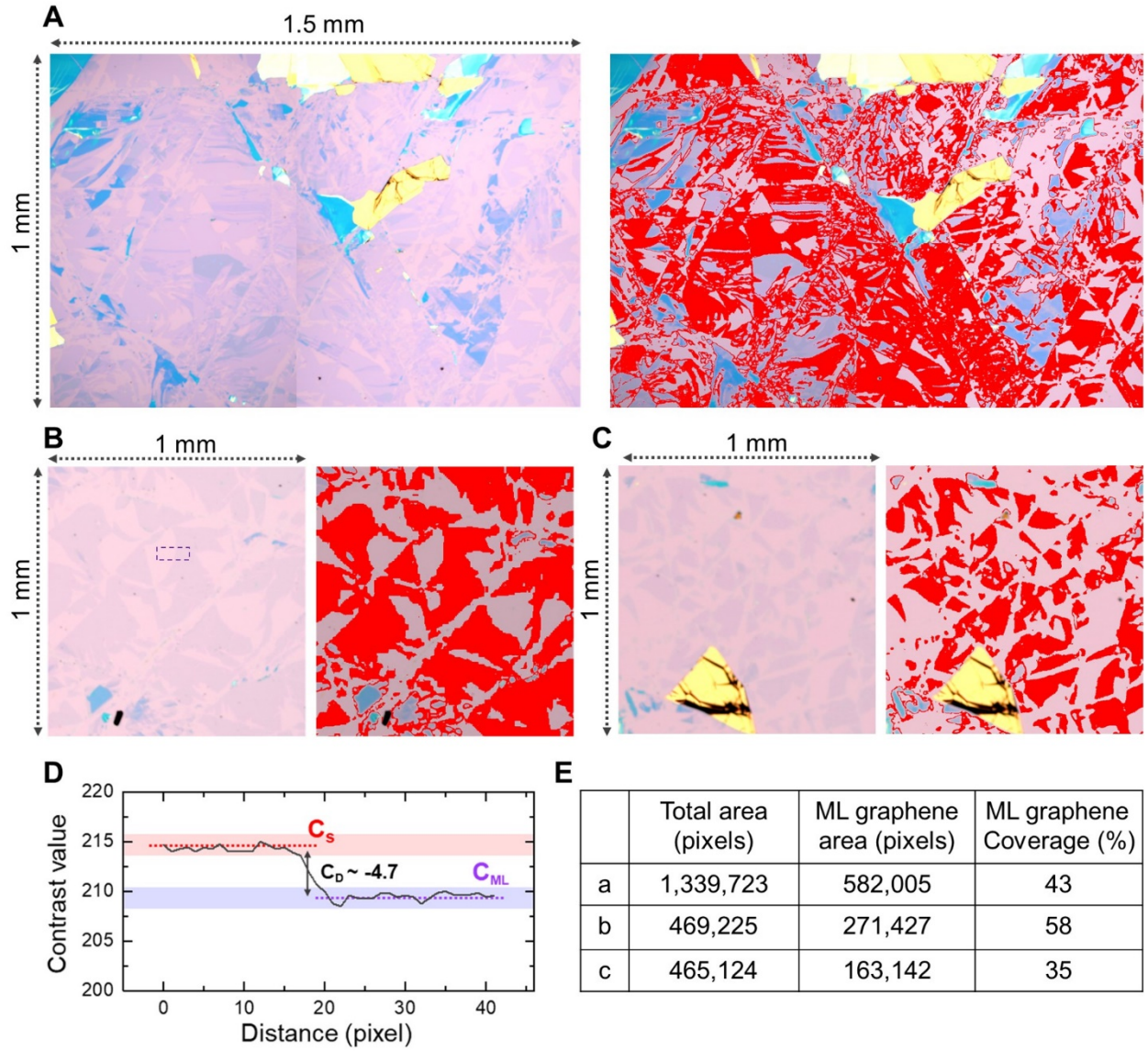

E

	Total area (pixels)	ML graphene area (pixels)	ML graphene Coverage (%)
a	1,339,723	582,005	43
b	469,225	271,427	58
c	465,124	163,142	35

Fig. S5 Monolayer coverage of LEE-graphene. (**A-C**) Representative OM images of LEE-graphene 1 x 1.5 mm^2 and 1 x 1 mm^2 in size and corresponding images in which the region of monolayer (ML) graphene is filled in red color. (**D**) Calculated optical contrast difference (C_D) of monolayer graphene (C_{ML}) with respect to the 300 nm SiO_2/Si substrate (C_S), which is approximately -4.7. Each pixel corresponding to monolayer graphene is marked in red in (**A-C**). (**E**) The coverage of monolayer graphene is calculated to be 43%, 58% and 35%.

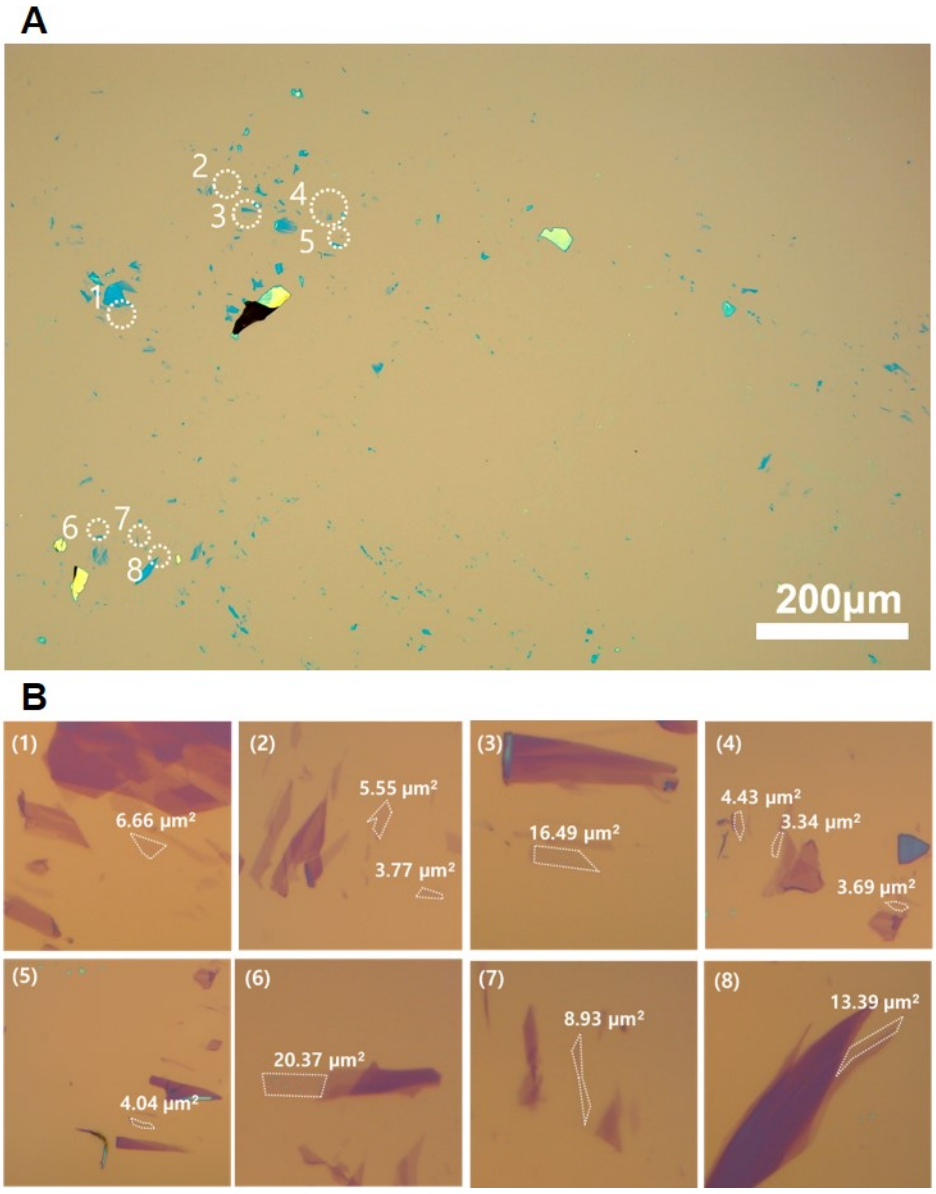

Fig. S6 Monolayer coverage for standard exfoliation. (**A**) OM image of an approximately 1 mm^2 area after standard exfoliation. Monolayer graphene exists in the dashed circular regions in the optical image. (**B**) High-magnification OM images of the circular regions. The size of individual monolayer graphene is also denoted in the images.

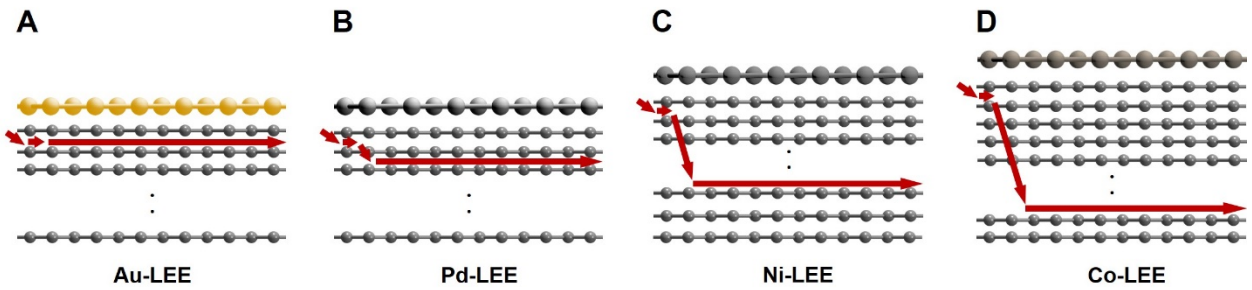

Fig. S7 Schematic illustration of the spalling path depending on the metal film. (**A-D**) As the increase of binding energy between metal and graphene, the spalling depth increase.

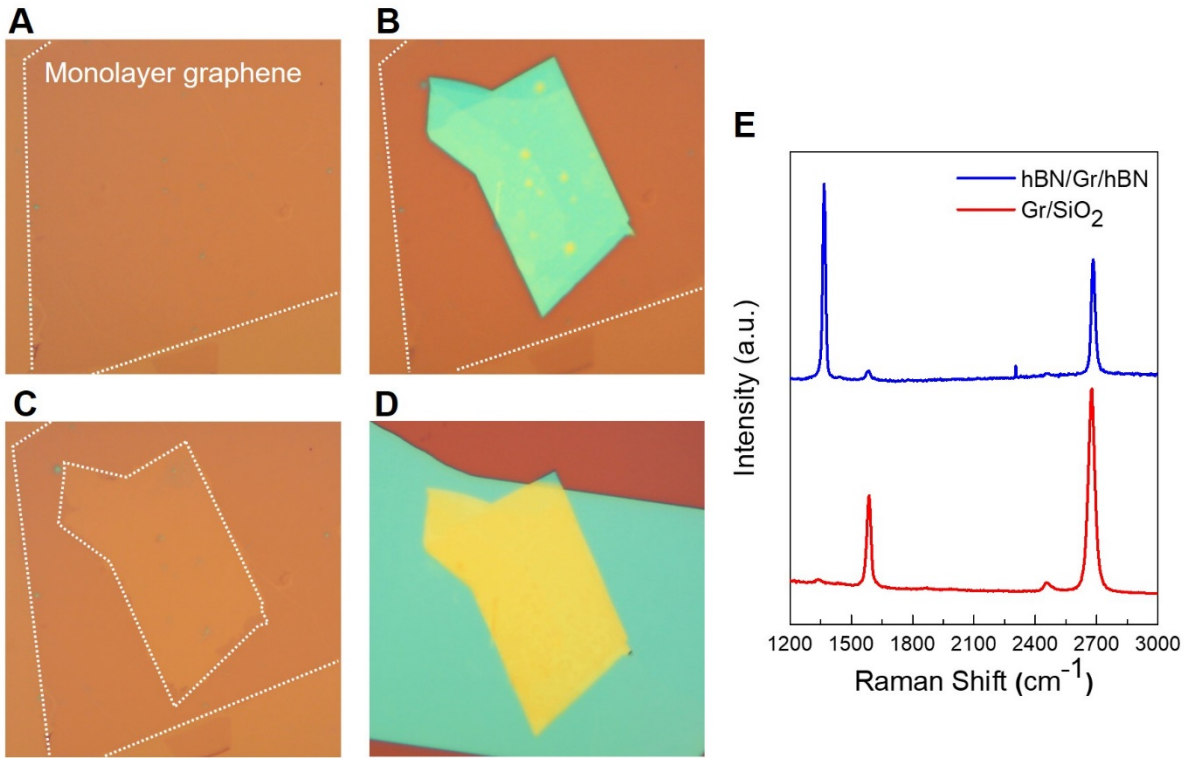

Fig. S8 hBN encapsulation process and Raman spectrum before/after encapsulation. (**A-D**) Monolayer graphene was prepared by the LEE method. The top hBN flake was dropped onto monolayer graphene, and the hBN/graphene stack was lifted up at 60 °C. Subsequently, we dropped the hBN/graphene stack onto the bottom hBN flake at 130 °C. (**E**) Representative Raman spectrum of monolayer graphene before and after encapsulation.

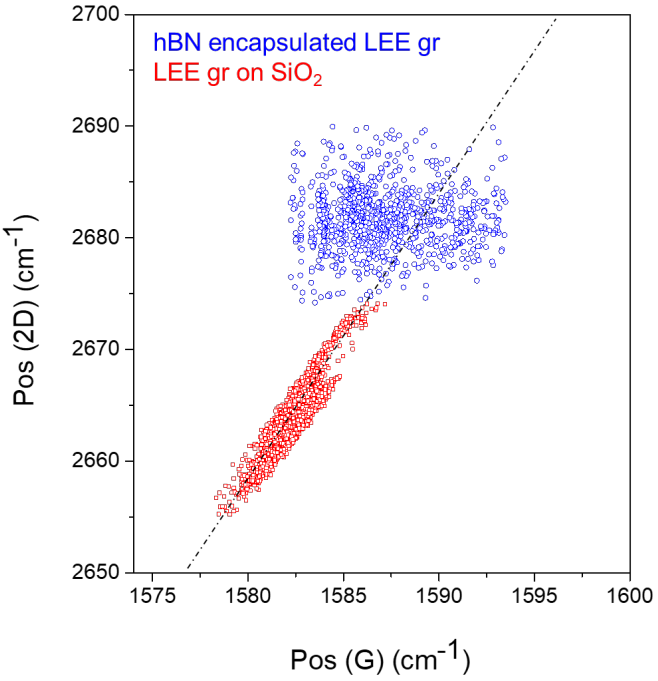

Fig. S9 Another data set of Raman spectroscopy. ω_{2D} versus ω_G recorded on two different samples: prepared by Au-LEE (red circles) and hBN encapsulation (blue circles).

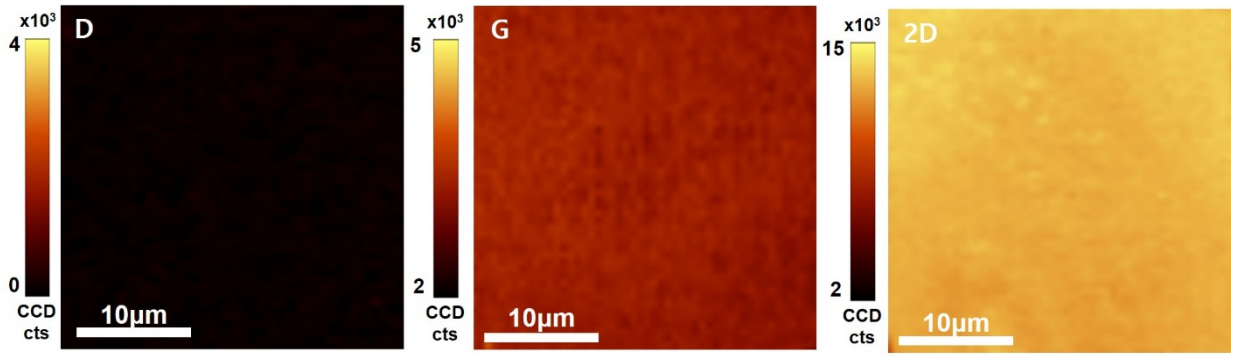

Fig. S10 Raman intensity mapping of LEE-graphene. Raman intensity mapping of the D peak (1350 cm^{-1}), G peak (1580 cm^{-1}) and 2D peak (2700 cm^{-1}) of monolayer graphene obtained by Au-LEE.

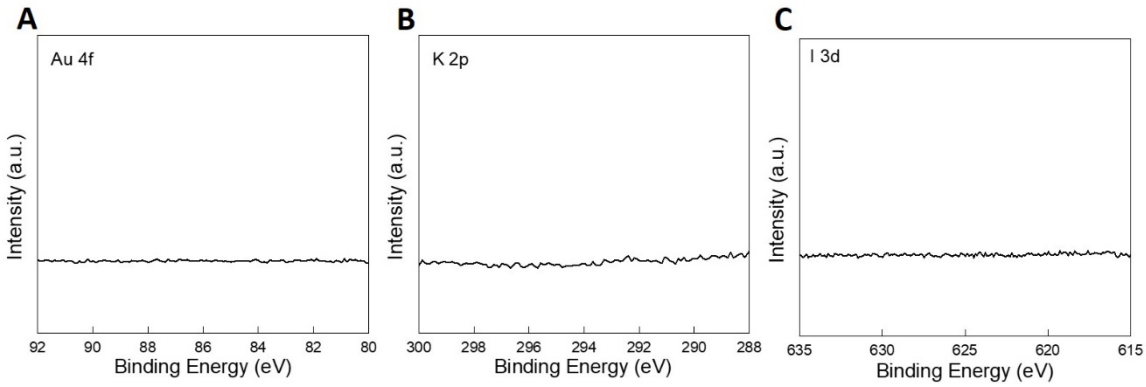

Fig. S11 XPS analysis of LEE-graphene. (**A-C**) Core-level peaks of Au 4f, K 2p and I 3d in the XPS spectrum of monolayer graphene obtained by Au-LEE. Peaks related to the Au and Au etchants (KI/I_2 solution) are not observed, which indicates that the stressor Au film was completely removed and that chemical residues from the Au etchant were fully washed away.

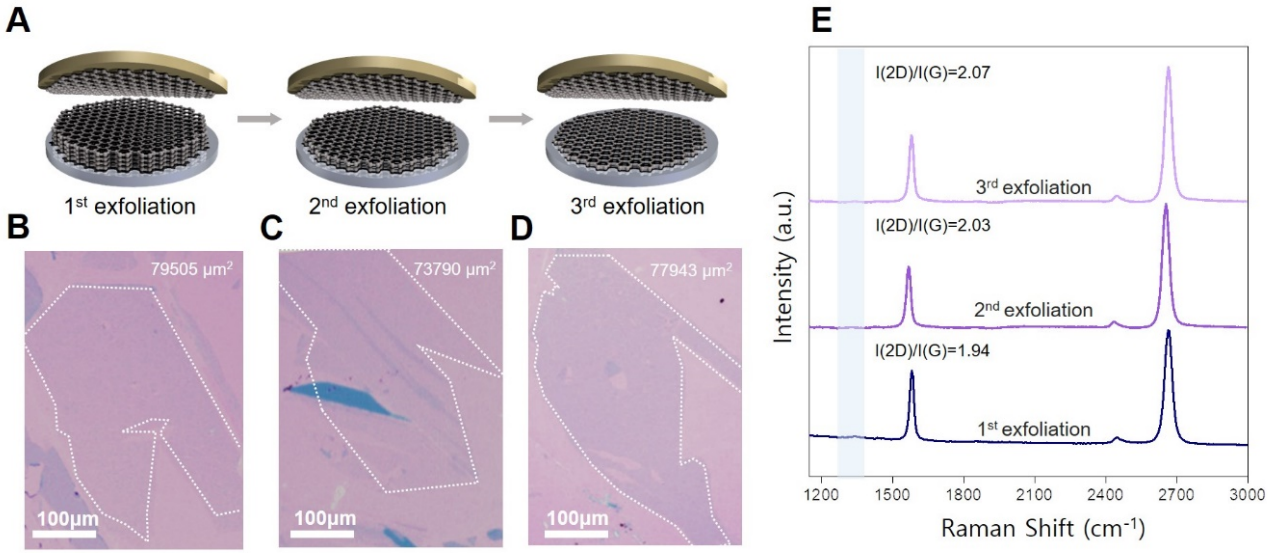

Fig. S12 Repeated exfoliation of large-area monolayer graphene. (**A**) Schematic illustration of the repeated LEE process. (**B-D**) Optical images of the large-area monolayer graphene on 300 nm-SiO_2/Si wafers obtained by the first, second, and third repeated LEE processes. (**E**) Raman spectra of three different graphene layers exfoliated from the same graphite flake.

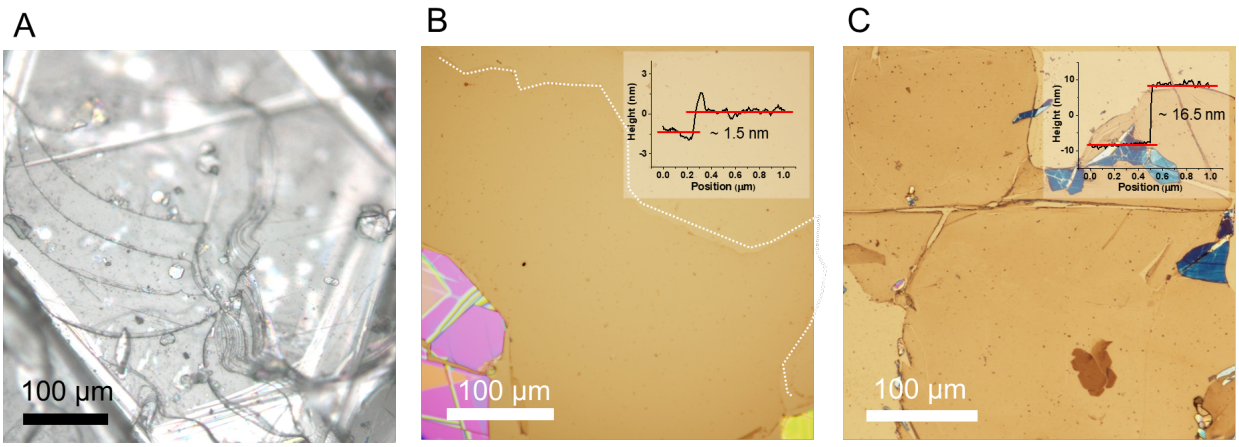

Fig S13. Layer engineered exfoliation for hBN. (A) OM image of hBN crystals. (B and C) OM images of layer-engineered hBN prepared by using Pd and Co. Interfacial toughness with hBN is ~170 meV and ~350 meV, respectively. Insets show that the thickness of each exfoliated hBN we obtained is 1.5 nm and 16 nm, respectively, with a lateral size of a few hundred μm (*42*).

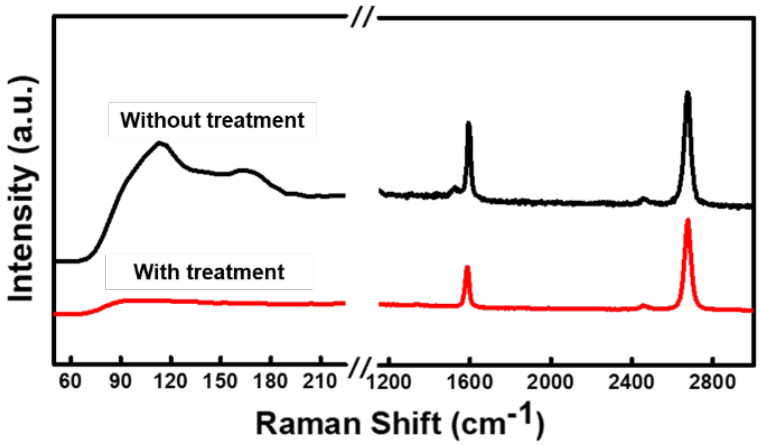

Fig. S14. Raman spectra of LEE-graphene before and after soaking treatment. The etchant related peaks are observed from LEE-graphene without soaking treatment (black) at lower wavelength region (110 and 160 cm^{-1}) which represent triiodide (I_3^-) and pentaiodide (I_5^-) but it disappeared from the LEE-graphene with soaking treatment (red) (*43*).

REFERENCES AND NOTES

1. K. S. Novoselov, A. K. Geim, S. V. Morozov, D. Jiang, Y. Zhang, S. V. Dubonos, I. V. Grigorieva, A. A. Firsov, Electric field effect in atomically thin carbon films. *Science* **306**, 666–669 (2004).

2. Y. Zhang, Y.-W. Tan, H. L. Stormer, P. Kim, Experimental observation of the quantum Hall effect and Berry's phase in graphene. *Nature* **438**, 201–204 (2005).

3. F. Wang, Y. Zhang, C. Tian, C. Girit, A. Zettl, M. Crommie, Y. R. Shen, Gate-variable optical transitions in graphene. *Science* **320**, 206–209 (2008).

4. Y. Zhu, S. Murali, M. D. Stoller, K. J. Ganesh, W. Cai, P. J. Ferreira, A. Pirkle, R. M. Wallace, K. A. Cychosz, M. Thommes, D. Su, E. A. Stach, R. S. Ruoff, Carbon-based supercapacitors produced by activation of graphene. *Science* **332**, 1537–1541 (2011).

5. X. Li, W. Cai, J. An, S. Kim, J. Nah, D. Yang, R. Piner, A. Velamakanni, I. Jung, E. Tutuc, S. K. Banerjee, L. Colombo, R. S. Ruoff, Large-area synthesis of high-quality and uniform graphene films on copper foils. *Science* **324**, 1312–1314 (2009).

6. K. S. Kim, Y. Zhao, H. Jang, S. Y. Lee, J. M. Kim, K. S. Kim, J.-H. Ahn, P. Kim, J.-Y. Choi, B. H. Hong, Large-scale pattern growth of graphene films for stretchable transparent electrodes. *Nature* **457**, 706–710 (2009).

7. J.-H. Lee, E. K. Lee, W.-J. Joo, Y. Jang, B.-S. Kim, J. Y. Lim, S.-H. Choi, S. J. Ahn, J. Ahn, M.-H. Park, C.-W. Yang, B. L. Choi, S.-W. Hwang, D. Whang, Wafer-scale growth of single-crystal monolayer graphene on reusable hydrogen-terminated germanium. *Science* **344**, 286–289 (2014).

8. A. O. Sboychakov, A. V. Rozhkov, A. L. Rakhmanov, F. Nori, Externally controlled magnetism and band gap in twisted bilayer graphene. *Phys. Rev. Lett.* **120**, 266402 (2018).

9. Y. Cao, V. Fatemi, S. Fang, K. Watanabe, T. Taniguchi, E. Kaxiras, P. Jarillo-Herrero, Unconventional superconductivity in magic-angle graphene superlattices. *Nature* **556**, 43–50 (2018).

10. C.-C. Lu, Y.-C. Lin, Z. Liu, C.-H. Yeh, K. Suenaga, P.-W. Chiu, Twisting bilayer graphene superlattices. *ACS Nano* **7**, 2587–2594 (2013).

11. K. M. Subhedar, I. Sharma, S. R. Dhakate, Control of layer stacking in CVD graphene under quasi-static condition. *Phys. Chem. Chem. Phys.* **17**, 22304–22310 (2015).

12. S. B. Desai, S. R. Madhvapathy, M. Amani, D. Kiriya, M. Hettick, M. Tosun, Y. Zhou, M. Dubey, J. W. Ager III, D. Chrzan, A. Javey, Gold-mediated exfoliation of ultralarge optoelectronically-perfect monolayers. *Adv. Mater.* **28**, 4053–4058 (2016).

13. M. Velický, G. E. Gonnelly, W. R. Hendren, S. McFarland, D. Scullion, W. J. I. DeBenedetti, G. C. Correa, Y. Han, A. J. Wain, M. A. Hines, D. A. Muller, K. S. Novoselov, H. D. Abruna, R. M. Bowman, E. J. G. Santos, F. Huang, Mechanism of gold-assisted exfoliation of centimeter-sized transition-metal dichalcogenide monolayers. *ACS Nano* **12**, 10463–10472 (2018).

14. J. Shim, S.-H. Bae, W. Kong, D. Lee, K. Qiao, D. Nezich, Y. J. Park, R. Zhao, S. Sundaram, X. Li, H. Yeon, C. Choi, H. Kum, R. Yue, G. Zhou, Y. Ou, K. Lee, J. Moodera, X. Zhao, J.-H. Ahn, C. Hinkle, A. Ougazzaden, J. Kim, Controlled crack propagation for atomic precision handling of wafer-scale two-dimensional materials. *Science* **362**, 665–670 (2018).

15. F. Liu, W. Wu, Y. Bai, S. H. Chae, Q. Li, J. Wang, J. Hone, X.-Y. Zhu, Disassembling 2D van der Waals crystals into macroscopic monolayers and reassembling into artificial lattices. *Science* **367**, 903–906 (2020).

16. J. Kim, H. Park, J. B. Hannon, S. W. Bedell, K. Fogel, D. K. Sadana, C. Dimitrakopoulos, Layer-resolved graphene transfer via engineered strain layers. *Science* **342**, 833–836 (2013).

17. M.-Y. He, J. W. Hutchinson, Crack deflection at an interface between dissimilar elastic materials. *Int. J. Solids Struct.* **25**, 1053–1067 (1989).

18. Z. Suo, J. W. Hutchinson, Steady-state cracking in brittle substrates beneath adherent films. *Int. J. Solids Struct.* **25**, 1337–1353 (1989).

19. G. Giovannetti, P. A. Khomyakov, G. Brocks, V. M. Karpan, J. van den Brink, P. J. Kelly, Doping graphene with metal contacts. *Phys. Rev. Lett.* **101**, 026803 (2008).

20. L. A. Girifalco, R. A. Lad, Energy of cohesion, compressibility, and the potential energy functions of the graphite system. *J. Chem. Phys.* **25**, 693–697 (1956).

21. M. C. Schabel, J. L. Martins, Energetics of interplanar binding in graphite. *Phys. Rev. B* **46**, 7185–7188 (1992).

22. Y. Huang, E. Sutter, N. N. Shi, J. Zheng, T. Yang, D. Englund, H.-J. Gao, P. Sutter, Reliable exfoliation of large-area high-quality flakes of graphene and other two-dimensional materials. *ACS Nano* **9**, 10612–10620 (2015).

23. Y. Huang, Y.-H. Pan, R. Yang, L.-H. Bao, L. Meng, H.-L. Luo, Y.-Q. Cai, G.-D. Liu, W.-J. Zhao, Z. Zhou, L.-M. Wu, Z.-L. Zhu, M. Huang, L.-W. Liu, L. Liu, P. Cheng, K.-H. Wu, S.-B. Tian, C.-Z. Gu, Y.-G. Shi, Y.-F. Guo, Z. G. Cheng, J.-P. Hu, L. Zhao, G.-H. Yang, E. Sutter, P. Sutter, Y.-L. Wang, W. Ji, X.-J. Zhou, H.-J. Gao, Universal mechanical exfoliation of large-area 2D crystals. *Nat. Commun.* **11**, 2453 (2020).

24. Z. Ni, Y. Wang, T. Yu, Z. Shen, Raman spectroscopy and imaging of graphene. *Nano Res.* **1**, 273–291 (2008).

25. J. Yan, Y. Zhang, P. Kim, A. Pinczuk, Electric field effect tuning of electron-phonon coupling in graphene. *Phys. Rev. Lett.* **98**, 166802 (2007).

26. C. Neumann, S. Reichardt, P. Venezuela, M. Drögeler, L. Banszerus, M. Schmitz, K. Watanabe, T. Taniguchi, F. Mauri, B. Beschoten, S. V. Rotkin, C. Stampfer, Raman spectroscopy as probe of nanometre-scale strain variations in graphene. *Nat. Commun.* **6**, 8429 (2015).

27. J. E. Lee, G. Ahn, J. Shim, Y. S. Lee, S. Ryu, Optical separation of mechanical strain from charge doping in graphene. *Nat. Commun.* **3**, 1024 (2012).

28. M. Mohr, J. Maultzsch, C. Thomsen, Splitting of the Raman 2*D* band of graphene subjected to strain. *Phys. Rev. B* **82**, 201409 (2010).

29. F. Ding, H. Ji, Y. Chen, A. Herklotz, K. Dörr, Y. Mei, A. Rastelli, O. G. Schmidt, Stretchable graphene: A close look at fundamental parameters through biaxial straining. *Nano Lett.* **10**, 3453–3458 (2010).

30. P. Nemes-Incze, Z. Osváth, K. Kamarás, L. P. Biró, Anomalies in thickness measurements of graphene and few layer graphite crystals by tapping mode atomic force microscopy. *Carbon* **46**, 1435–1442 (2008).

31. Z. Zhang, J. Du, D. Zhang, H. Sun, L. Yin, L. Ma, J. Chen, D. Ma, H.-M. Cheng, W. Ren,Rosin-enabled ultraclean and damage-free transfer of graphene for large-area flexible organic light-emitting diodes. *Nat. Commun.* **8**, 14560 (2017).

32. J.-Y. Moon, S.-I. Kim, S.-K. Son, S.-G. Kang, J.-Y. Lim, D. K. Lee, B. Ahn, D. Whang,H. K. Yu, J.-H. Lee, An eco-friendly, CMOS-compatible transfer process for large-scale CVD-graphene. *Adv. Mater. Interfaces* **6**, 1900084 (2019).

33. L. Wang, I. Meric, P. Y. Huang, Q. Gao, Y. Gao, H. Tran, T. Taniquchi, K. Watanabe, L. M. Campos, D. A. Muller, J. Guo, P. Kim, J. Hone, K. L. Shepard, C. R. Dean, One-dimensional electrical contact to a two-dimensional material. *Science* **342**, 614–617 (2013).

34. M. Yankowitz, Q. Ma, P. Jarillo-Herrero, B. J. LeRoy, Van der waals heterostructures combining graphene and hexagonal boron nitride. *Nat. Rev. Phys.* **1**, 112–125 (2019).

35. J.-H. Chen, C. Jang, S. Adam, M. S. Fuhrer, E. D. Williams, M. Ishigami, Charged-impurity scattering in graphene. *Nat. Phys.* **4**, 377–381 (2008).

36. N. J. G. Couto, D. Costanzo, S. Engels, D.-K. Ki, K. Watanabe, T. Taniguchi, C. Stampfer, F. Guinea, A. F. Morpurgo, Random strain fluctuations as dominant disorder source for high-quality on-substrate graphene devices. *Phys. Rev. X.* **4**, 041019 (2014).

37. J. Crossno, J. K. Shi, K. Wang, X. Liu, A. Harzheim, A. Lucas, S. Sachdev, P. Kim, T. Taniguchi, K. Watanabe, T. A. Ohki, K. C. Fong, Observation of the Dirac fluid and the breakdown of the Wiedemann-Franz law in graphene. *Science* **351**, 1058–1061 (2016).

38. J.-H. Chen, C. Jang, S. Xiao, M. Ishigami, M. S. Fuhrer, Intrinsic and extrinsic performance limits of graphene devices on SiO_2. *Nat. Nanotechnol.* **3**, 206–209 (2008).

39. C. R. Dean, A. F. Young, I. Meric, C. Lee, L. Wang, S. Sorgenfrei, K. Watanabe, T. Taniguchi, P. Kim, K. L. Shepard, J. Hone, Boron nitride substrates for high-quality graphene electronics. *Nat. Nanotechnol.* **5**, 722–726 (2010).

40. F. Pizzocchero, L. Gammelgaard, B. S. Jessen, J. M. Caridad, L. Wang, J. Hone. P. Bøggild, T. J. Booth, The hot pick-up technique for batch assembly of van der Waals heterostructures. *Nat. Commun.* **7**, 11894 (2016).

41. H. Li, J. Wu, X. Huang, G. Lu, J. Yang, X. Lu, Q. Xiaong, H. Zhang, Rapid and reliable thickness identification of two-dimensional nanosheets using optical microscopy. *ACS Nano* **7**, 10344–10353 (2013).

42. M. Bokdam, G. Brocks, M. I. Katsnelson, P. J. Kelly, Schottky barriers at hexagonal boron nitride/metal interfaces: A first-principles study. *Phys. Rev. B* **90**, 085415 (2014).

43. G. Kalita, K. Wakita, M. Takahashi, M. Umeno, Iodine doping in solid precursor-based CVD growth graphene film. *J. Mater. Chem.* **21**, 15209–15213 (2011)